Hindawi
Advances in Materials Science and Engineering
Volume 2019, Article ID 8562102, 7 pages
https://doi.org/10.1155/2019/8562102

Research Article

Computational Assessment of Thermal Conductivity of Compacted Graphite Cast Iron

Yue Wu, Jianping Li, Zhong Yang, Zhijun Ma, Yongchun Guo, Dong Tao, Tong Yang, and Minxian Liang

Shaanxi Province Engineering Research Centre for Aluminium/Magniesum Light Alloy and Composites, School of Materials and Chemical Engineering, Xi'an Technological University, Xi'an 710021, China

Correspondence should be addressed to Jianping Li; lunwenljp@163.com

Received 1 November 2018; Revised 25 January 2019; Accepted 7 February 2019; Published 1 April 2019

Academic Editor: Patrice Berthod

Two-dimensional FE models of CGI with different pearlite contents for thermal conductivity analysis were established according to the real metallographic images obtained by Pro/E and ANSYS. Meanwhile, thermal conductivity of CGI with different pearlite contents was tested through the laser flash method. It is indicated that the thermal conductivity of CGI declines with the increase of pearlite. When pearlite is increased from 10% to 80%, the experimental values decline from 46.63 W/m·K to 36.86 W/m·K, reducing by 21%. However, this declining tendency becomes gentle and slight when pearlite is more than 40%. In addition, the calculation results with the consideration of interfacial contact thermal conductance (ICTC) and pearlite are much close to experimental values; especially when pearlite is 80%, the difference between them is only about 2%. It can be concluded that the FE models are convenient and reasonable to analyze thermal conductivity of CGI.

1. Introduction

As a preferred material for engine components at high temperature, such as cylinder head, compacted graphite cast iron (CGI) exhibits a super combination of excellent mechanical properties and outstanding thermal conductivity [1, 2]. With the increase in power density, the cylinder head material endures very high temperature; therefore, the material needs superior thermal conductivity in order to transfer the heat quickly and avoid thermomechanical deformation [3–5].

It is generally accepted that graphite has the best thermal conductivity in cast iron. According to data [6, 7], thermal conductivity of graphite along the prism planes at room temperature is 5.7 W/m·K, while the value along basal planes is 1950 W/m·K. When graphite grows along the basal planes preferentially, it becomes lamellar and constitutes eutectic cells, which build 3D structure and make heat to spread through graphite eutectic cells quickly. When graphite grows along the *c*-axis direction preferentially, it is spherical and distributes in the matrix separately, which leads to poor connectivity between graphite particles and compel most of the heat to pass through the matrix [8, 9]. Although the growth direction of vermicular graphite is a mess, graphite is mainly along basal planes and particles gather as eutectic cells, which makes better heat conduction than that of nodular graphite [10].

Recently, many researches have analyzed the thermal conductivity of cast iron. Holmgren et al. [11] estimated the relationship between graphite growth direction and thermal conductivity of cast iron. They pointed out that thermal conductivity of flake graphite is better than that of vermicular graphite followed by that of nodular graphite because heat diffuses faster in the *a*-axis direction of graphite than that in the *c*-axis direction. Although chunky graphite has large interconnected eutectic cells, there is no beneficial effect on heat transferring due to its *c*-axis direction of hexagonal crystal. Hecht et al. [12] also found out the thermal diffusivity of cast iron increases with size of A-type flake graphite. However, these studies mainly focused on experiments to analyze thermal conductivity of cast iron, which consumes much time and it is difficult to represent

heat conduction process vividly. There are many models to calculate thermal conductivity, such as Helsing model [13, 14], Maxwell model, Bruggeman model, and Hasin–Shtrikman model [15], which are convenient to calculate and apply. But these models only suit cast iron with ferric matrix. Modern engine materials need excellent mechanical property, which needs pearlite, a reinforced phase, to enhance the cast iron strength. Because of pearlite, thermal conductivity of matrix decreases. Therefore, above models are no longer inadequate. Recently, finite element (FE) simulation has been used for analyzing the thermal conductivity of cast iron [16, 17]. It is a feasible technical method. Ma [17] pointed out that thermal conductivity of CGI increases with vermicularity through FE simulation. The calculation values are close to reality when considering interfacial contact thermal conductance (ICTC).

To our best knowledge, thermal conductivity of CGI analysis through the FE method and data with different pearlite contents are rare and scarce. Therefore, it is great indispensable to discern the variation of thermal conductivity of CGI with different pearlite contents. In the present study, there are two purposes: (1) attempting to build a two-dimensional heat conduction model of CGI by using FE methods and (2) analyzing the influence of pearlite and ICTC on the thermal conductivity of CGI.

2. Building of FE Models

Microstructure of cast iron was observed by using a Nicon300 metallographic microscope and was traced by using Pro/E. Then an IGES file was generated and imported into ANSYS to establish the FE models [16, 17]. Cast iron material can be seen as a kind of composite material [14, 18, 19]. Graphite, ferrite, and pearlite can been seen as three phases in the microstructure. Thermal Solid Quad 8 node PLANE77 element is used to mesh the physical model. The meshes along the interface between graphite and casting matrix are more refined in order to increase the accuracy of calculations.

2.1. FE Models with Different Graphite Morphologies. FE models with three graphite morphologies (lamellar, vermicular, and nodular) were built, respectively, according to the microstructure, as shown in Figure 1. The corresponding FE model of grey iron is shown in Figure 2.

2.2. FE Models of CGI with Different Pearlite Contents. The metallographic specimen after etching by using 4% nital solution was observed with an optical microscope, and the area percentages of pearlite were measured by using DT 2000 metallographic software. Figures 3(a), 3(c), 3(e), 3(g), and 3(i) present the microstructure of CGI with pearlite contents from 10% to 80%, respectively. Figures 3(b), 3(d), 3(f), 3(h), and 3(j) present the corresponding FE models. For simplicity, it is assumed that graphite is an isotropic material and its thermal conductivity is set as 130 W/m·K [20]. In addition, ignoring solid solution of alloying elements in matrix, thermal conductivity values of ferrite and pearlite are regarded as 78.5 W/m·K [21] and 52 W/m·K, respectively [22].

2.3. Boundary Conditions. Under the steady condition, three types of boundary conditions can be used to simulate the heat transfer problems:

The first one is that temperature on the boundary of T_x is fixed and the simple case is that T_x is constant:

$$T_x = \text{const.} \tag{1}$$

The second one is that heat flux on the boundary is fixed and the simple case is that heat flux is constant:

$$-k\left(\frac{\partial T}{\partial n}\right)_w = \text{const}, \tag{2}$$

where n is the normal direction of the surface and k is the thermal conductivity.

The third one is that the heat transfer coefficient and the surrounding temperature between boundary and surrounding are fixed. In this paper, the first and third types of boundary conditions are used in the calculation. The upper and lower sides of the FE model are set up adiabatic. Convective heat transfer and fixed temperature boundary condition are defined on the left and right sides of the model, respectively.

According to the Fourier law of heat conduction, heat conduction is directly proportional to the temperature gradient, heat transfer area, and time. It can be expressed by equation (3); therefore, the thermal conductivity k can be calculated by equation (4):

$$\phi = -kA\frac{dT}{dx}, \tag{3}$$

$$k = \frac{\phi/A}{dT/dx}, \tag{4}$$

where Φ is the heat flux, A is the heat conduction area, and dT/dx is the temperature gradient. The heat flux Φ is a constant in the two-dimensional FE model of this paper. Therefore, the heat flux density q can be expressed by (5). The heat flux q can be calculated by equations (6) and (7):

$$q = -k\frac{dT}{dx}, \tag{5}$$

$$\int q \cdot dx = \int -k \cdot dT, \tag{6}$$

$$q \cdot L = -k \cdot \Delta T, \tag{7}$$

where L is the length of the FE model in the direction of heat conduction and ΔT is the temperature difference from the left side to right side of the FE model. Heat flux q, length of FE model L, and temperature difference ΔT can be obtained through FE calculation results. Hence, the thermal conductivity k can be calculated according to the following equation:

$$k = -\frac{qL}{\Delta T}. \tag{8}$$

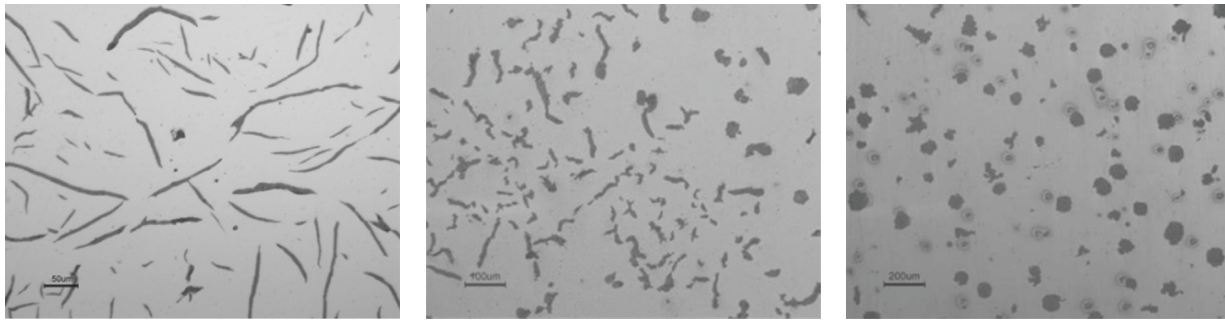

(a) (b) (c)

Figure 1: Microstructure of cast iron: (a) grey iron; (b) compacted graphite iron; (c) nodular graphite iron.

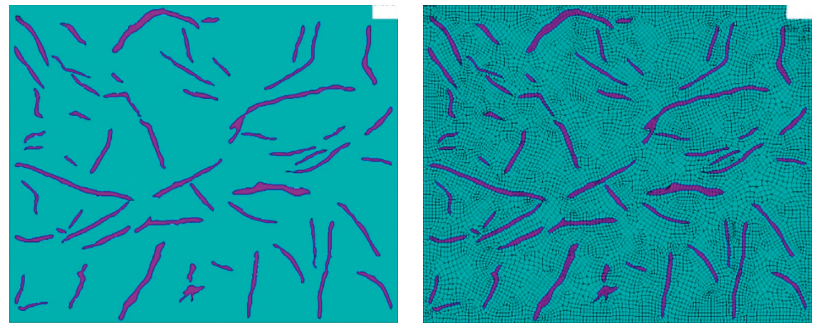

(a) (b)

Figure 2: (a) FE model of grey iron; (b) meshing model.

2.4. Interfacial Contact Thermal Conductance (ICTC). According to Yang et al. [16], ICTC can be seen as a thermal barrier resistance between diamond and aluminium matrix. Ma [17, 19] pointed out that interfacial thermal conductance cannot be ignored in the analysis of heat conduction. As ascribed in the former section, CGI can be seen as a simple composite material. Therefore, ICTC was established in the FE models of this paper, as shown in Figure 4. The value of ICTC was set as 0.1×10^6 W/m^2·K.

3. Thermal Conductivity Test

Thermal conductivity can be tested by using the laser flash method. Firstly, thermal diffusion coefficient of CGI was measured by using the NETZSCH LFA type 457 unsteady laser thermal conductivity meter as described in the following equation:

$$\alpha = C \cdot \frac{l^2}{t_{0.5}}, \tag{9}$$

where α is the thermal diffusion coefficient, l is the thickness of the specimen, $C = 0.1388$, and $t_{0.5}$ is the time that the sample temperature on the back rise 50%.

According to equation (10), thermal conductivity can be calculated:

$$\lambda = \alpha \rho C_P, \tag{10}$$

where λ is the thermal conductivity, ρ is the density, and C_P is the specific heat. The specific heat of material can be calculated by the following equation:

$$C_P = \frac{C_{PR} \cdot m_R \cdot \Delta T_R}{m_P \Delta T_P}, \tag{11}$$

where C_p and C_{PR} are the specific heat of the test sample and reference sample, respectively; m_p and m_R are the masses of the test sample and reference sample, respectively; and ΔT_P and ΔT_R are the temperature changes of the test sample and reference sample, respectively. The density of samples is measured by using the hydrostatic method, and mass and volume of the sample are measured by using the METTLER TOLEDO balance.

4. Results and Discussion

4.1. Effect of Graphite Morphologies on Thermal Conductivity. Figure 5 shows the distribution of temperature and heat flux of the grey cast iron. It can be seen that the temperature decreases from left to right in the model, and the temperature field is relatively homogeneous. Due to excellent thermal conductivity, heat flux of graphite is higher than that of matrix, which indicates that the heat transmission would pass through the graphite preferentially.

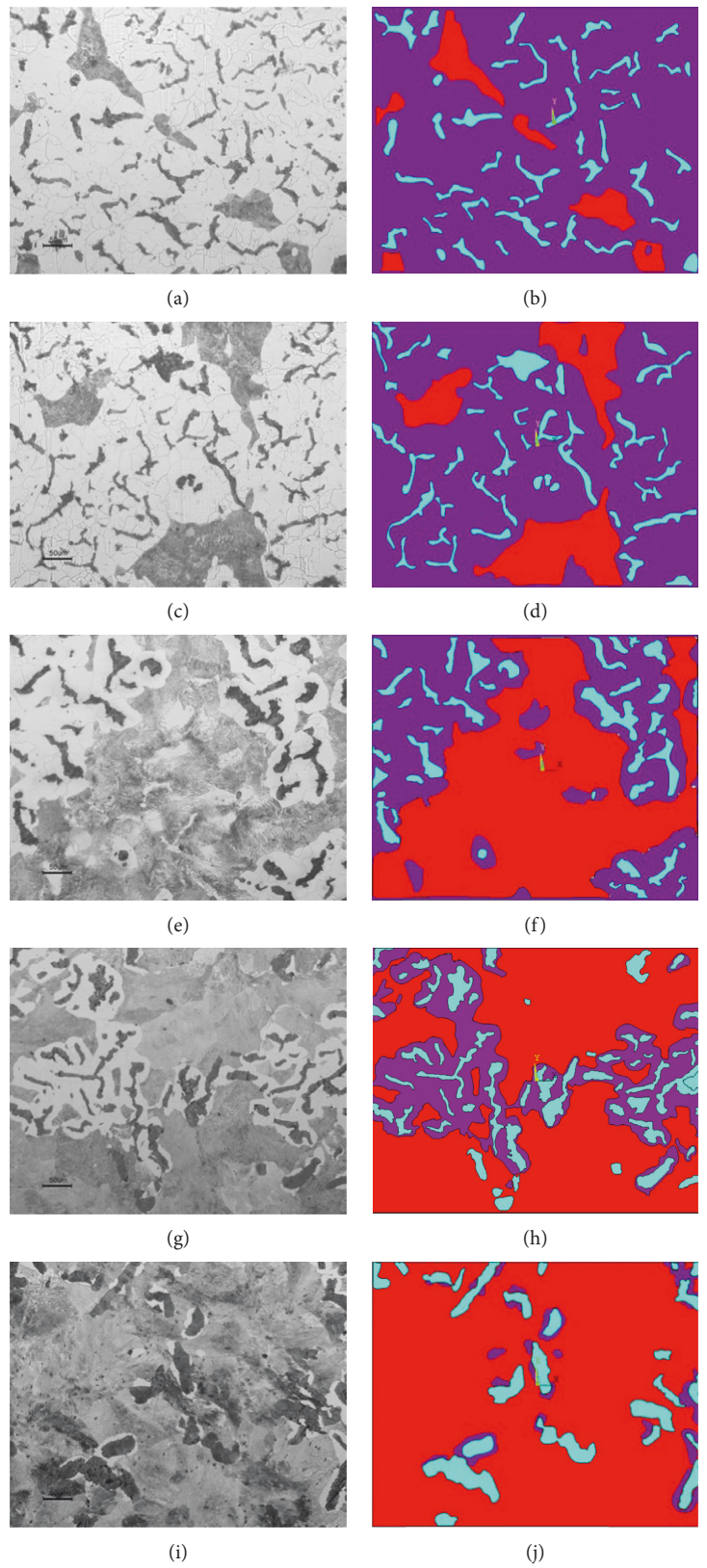

Figure 3: Microstructure of CGI and corresponding FE model with different pearlite contents. Microstructure: (a) 10%; (c) 20%; (e) 40%; (g) 60%; (i) 80%; FE models: (b) 10%, (d) 20%, (f) 40%, (h) 60%, (j) 80%.

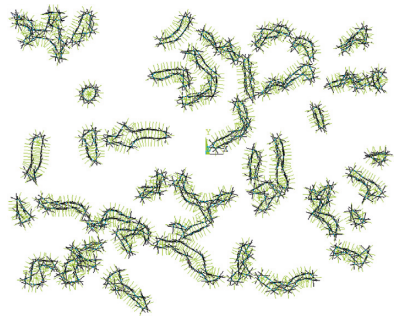

Figure 4: Interfacial model.

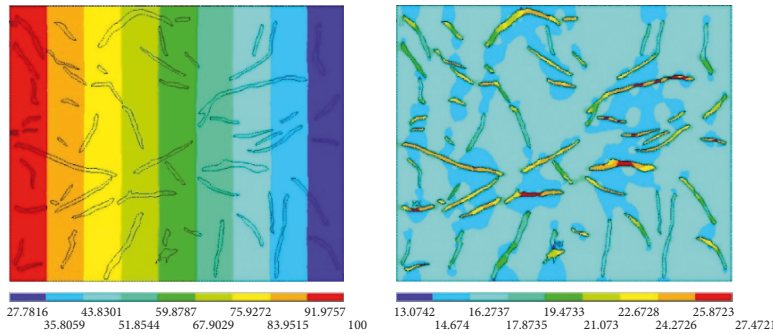

(a) (b)

Figure 5: The results of grey iron model: (a) temperature; (b) heat flux.

Table 1 shows the calculated thermal conductivity in different graphite morphologies. It can be seen that the values in three graphite morphologies are relatively close and the difference between them is only about 0.13% to 0.17%. Meanwhile, the calculated values are obviously greater than the actual thermal conductivity of cast irons (about 37–53 W/m·K). There are some reasons that can explain the large error. Firstly, the matrix of models is ferrite. It has the second best thermal conductivity in the microstructure. There is little obstruction during heat spread through matrix. FE models are different from reality because pearlite is out of consideration. Secondly, anisotropy of graphite is ignored. For simplicity, an assumption was made in simulation. Graphite can be seen as an isotropic material, and thermal conductivity value was set as 130 W/m·K. However, nodular graphite mainly grows along the *c*-axis direction, and the thermal conductivity value is only about 5.7 W/m·K. Hence, the thermal conductivity of nodular graphite iron is amplified virtually during simulation. Thirdly, ICTC was out of consideration in the FE model, which has a negative effect on heat conduction, as described by Ma and Yang. From the above analysis, calculation results are much higher than reality.

4.2. Effect of ICTC and Pearlite on Thermal Conductivity of CGI. In order to make the FE models more close to the actual situation, pearlite and ICTC were applied.

Table 1: Calculation values in different graphite morphologies (W/m·K).

Graphite shape	Lamellar	Compacted	Nodular
Thermal conductivity	83.25	83.14	83.28

Temperature distribution and heat flux with 10% pearlite of CGI without consideration of ICTC and with consideration of ICTC are described in Figures 6 and 7, respectively. It can be seen that temperature field and heat flux become uneven and irregular when ICTC is applied. Heat conduction in the matrix increases, and the efficiency of heat passing through the matrix is greater than that of without consideration of ICTC.

Thermal conductivity of CGI with different pearlite contents is described in Figure 8. It can be seen that the thermal conductivity of CGI decreases with increase in pearlite. When pearlite is increased from 10% to 80%, experimental values decline from 46.63 W/m·K to 36.86 W/m·K, reducing by 21%. In contrast, FE simulation results without consideration of ICTC decline from 81.32 W/m·K to 56.70 W/m·K, reducing by 30% and thermal conductivity values with consideration of ICTC declines from 54.78 W/m·K to 38.87 W/m·K, reducing by 29%.

Thermal conductivity decline is obvious and evident when pearlite is less than 40%. However, this declining tendency becomes slight when pearlite is more than 40%.

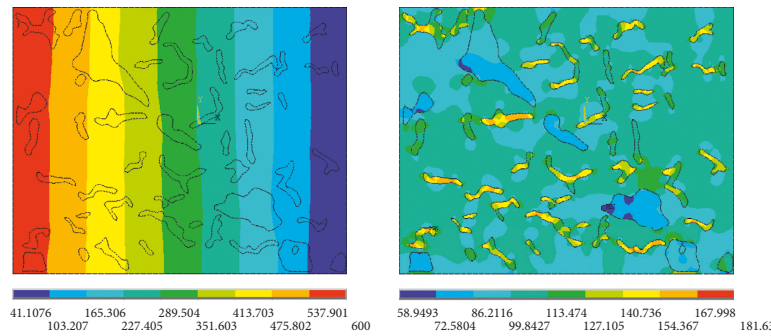

Figure 6: FE models with 10% pearlite without consideration of ICTC: (a) temperature field; (b) heat flux.

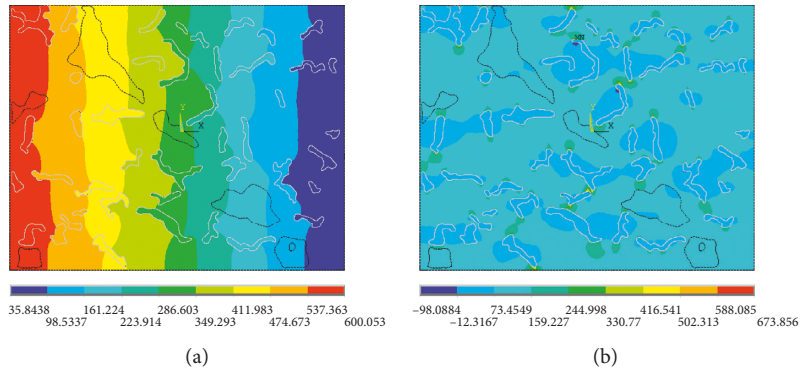

Figure 7: FE models with 10% pearlite with consideration of ICTC: (a) temperature field; (b) heat flux.

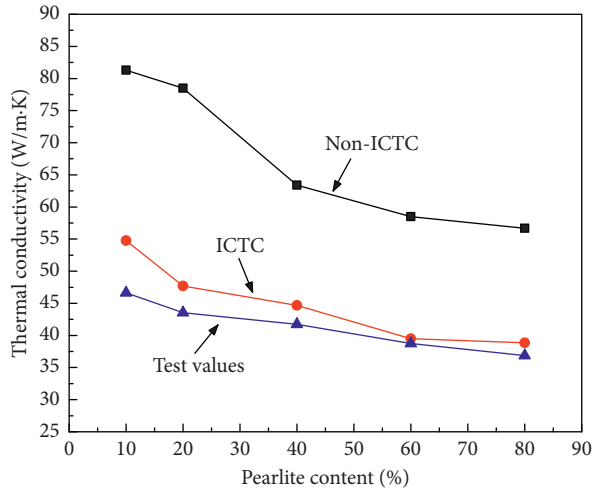

Figure 8: Thermal conductivity of CGI with different pearlite contents.

This phenomenon implies that the negative influence of pearlite in heat conduction recedes with increase of pearlite.

In addition, calculation results without consideration of ICTC are much higher than test results and difference between them is about 33.8% to 39.3%. When pearlite and ICTC are applied in the models at the same time, the calculation results are relatively close to the test values; especially when pearlite is 80%, the difference between them is only about 2%. It proves that application of ICTC and pearlite in models is reasonable.

5. Conclusions

(1) A two-dimensional heat conduction model of cast iron is established by Pro/E and ANSYS based on real metallographic images in this paper. The calculation results are close to the test values, which prove that FE simulation is a reasonable and convenient method to solve thermal conductivity of CGI.

(2) ICTC and pearlite are important factors in heat conduction of cast iron. Without considering ICTC, the calculated results are much higher than experimental values. The difference between them is about 33.8% to 39.3%. When pearlite and ICTC are applied in the FE models at the same time, the FE simulation results are much close to the experimental values; especially when pearlite is 80%, the difference between them is only about 2%.

(3) Thermal conductivity of CGI descends obviously and dramatically with the increase of pearlite when

pearlite is less than 40%; however, it becomes slight as pearlite is more than 40%. The negative influence on thermal conductivity reduces with the increase of pearlite.

Data Availability

The data used to support the findings of this study are available from the corresponding author upon request.

Conflicts of Interest

The authors declare that they have no conflicts of interest.

Acknowledgments

The authors would like to thank the National Basic Science Development Foundation of China (61322402) and Key Research Program of Shaanxi Provincial Department of Technology and Science (2018ZDXM-GY-137) for their financial support.

References

[1] S. Ghodrat, T. A. C. riemslag, L. A. I. kestens, R. H. Petrov, M. Janssen, and J. Sietsma, "Effects of holding time on thermomechanical fatigue properties of compacted graphite iron through tests with notched specimens," *Metallurgical and Materials Transactions A*, vol. 44, no. 5, pp. 2121–2130, 2013.

[2] T. Yang, Y. C. Guo, J. P. Li et al., "Microstructure and mechanical properties of thin-section compacted graphite cast iron," *Foundry*, vol. 57, no. 3, pp. 270–273, 2008.

[3] T. Matsushita, E. Ghassemali, A. Saro, L. Elmquist, and A. Jarfors, "On thermal expansion and density of CGI and SGI cast irons," *Metals*, vol. 5, no. 2, pp. 1000–1019, 2015.

[4] S. Dawson, "Compacted graphite iron-a material solution for modern diesel engine cylinder blocks and heads," *China Foundry*, vol. 6, no. 3, p. 241, 2009.

[5] Y. Wu, J. Li, Z. Yang et al., "Creep behavior accompanying oxidation of compacted graphite cast iron," *Materials Science and Engineering: A*, vol. 723, pp. 174–181, 2018.

[6] D. Holmgren, A. Diószegi, and I. L. Svensson, "Effects of nodularity on thermal conductivity of cast iron," *International Journal of Cast Metals Research*, vol. 20, no. 1, pp. 30–40, 2007.

[7] A. Velichko and F. Mücklich, "Shape analysis and classification of irregular graphite morphology in cast iron," *Carbohydrate Research*, vol. 339, no. 5, pp. 967–973, 2006.

[8] M. Selin and M. König, "Regression analysis of thermal conductivity based on measurements of compacted graphite irons," *Metallurgical and Materials Transactions A*, vol. 40, no. 13, pp. 3235–3244, 2009.

[9] O. Maluf, M. Angeloni, D. B. V. Castro, W. W. Bose Filho, D. Spinelli, and C. O. F. T. Ruckert, "Effect of alloying elements on thermal diffusivity of gray cast iron used in automotive brake disks," *Journal of Materials Engineering and Performance*, vol. 18, no. 7, pp. 980–984, 2009.

[10] H. Daniel, D. Attila, L. Ingvar et al., "Effects of carbon content and solidification rate on thermal conductivity of grey cast iron," *China Foundry*, vol. 4, no. 3, pp. 210–214, 2007.

[11] D. Holmgren, R. Källbom, and I. L. Svensson, "Influences of the graphite growth direction on the thermal conductivity of cast iron," *Metallurgical and Materials Transactions A*, vol. 38, no. 2, pp. 268–275, 2007.

[12] R. L. Hecht, R. B. Dinwiddie, and H. Wang, "The effect of graphite flake morphology on the thermal diffusivity of gray cast irons used for automotive brake discs," *Journal of Materials Science*, vol. 34, no. 19, pp. 4775–4781, 1999.

[13] J. Helsing and A. Helte, "Effective conductivity of aggregates of anisotropic grains," *Journal of Applied Physics*, vol. 69, no. 6, pp. 3583–3588, 1991.

[14] J. Helsing and G. Grimvall, "Thermal conductivity of cast iron: models and analysis of experiments," *Journal of Applied Physics*, vol. 70, no. 3, pp. 1198–1206, 1991.

[15] T. Matsushita, A. G. Saro, L. Elmquist, and A. E. W. Jarfors, "On the thermal conductivity of CGI and SGI cast irons," *International Journal of Cast Metals Research*, vol. 31, no. 3, pp. 135–143, 2017.

[16] W. L. Yang, K. Peng, L. P. Zhou, J. Zhu, and D. Li, "Finite element simulation and experimental investigation on thermal conductivity of diamond/aluminium composites with imperfect interface," *Computational Materials Science*, vol. 83, pp. 375–378, 2013.

[17] Z. J. Ma, Q. Wen, P. H. Gao et al., "Experimental assessment of interfacial contact thermal conductance between graphite and matrix in cast iron," *International Journal of Cast Metals Research*, vol. 31, no. 4, pp. 230–236, 2018.

[18] A. Rape, K. Gott, A. Kulkarni, and J. Singh, "Simulation of matrix conductivity in copper-diamond composites sintered by field assisted sintering technology," *Computational Materials Science*, vol. 110, pp. 29–33, 2015.

[19] Z. J. Ma, D. Tao, Z. Yang et al., "The effect of vermicularity on the thermal conductivity of vermicular graphite cast iron," *Materials & Design*, vol. 93, pp. 418–422, 2016.

[20] G. Ljustina, R. Larsson, and M. Fagerström, "Rate sensitive continuum damage models and mesh dependence in finite element analyses," *The Scientific World Journal*, vol. 2014, pp. 1–8, 2014.

[21] A. Velichko, A. Wiegmann, and F. Mücklich, "Estimation of the effective conductivities of complex cast iron microstructures using FIB-tomographic analysis," *Acta Materialia*, vol. 57, no. 17, pp. 5023–5035, 2009.

[22] H. Y. Fan, W. Li, and Z. H. Tang, "The influence of constitutes on thermal conductivity of cast irons," *Hot Working Technology*, vol. 5, pp. 49–51, 1999.